A study of Sensorless Control of Induction Motor at Zero Speed Utilizing High Frequency Voltage Injection

Dušan Drevenšek
University of Maribor, Faculty of Electrical Engineering and Computer Science
Smetanova 17, 2000 Maribor, Slovenia
Phone: +386 2 220 7309, Fax: +386 2 220 7315
e-mail: dusan.drevensek@uni-mb.si

Damir Žarko, Thomas A. Lipo
University of Wisconsin – Madison
Department of Electrical and Computer Engineering
2557 Engineering Hall, 1415 Engineering Drive
Madison, WI 53706-1691, USA
Phone: +1 608 262 0287, Fax: +1 608 262 5559
e-mail: zarko@cae.wisc.edu, lipo@engr.wisc.edu

Keywords

Sensorless control, induction motors, measurements, modelling

Abstract

A detailed investigation of sensorless control of induction motor at zero and very low speed based on injection of a pulsating high frequency voltage signal is presented. A sensing technique used to measure air gap flux position in a squirrel cage induction motor is based on the secondary effect of magnetic spatial nonlinearity caused by saturation of the stator laminations. The physical insight into the motor excited by high frequency test signals is given by means of experiment and finite element simulation. It is shown that it is possible to control the motor torque using the proposed technique, but with low bandwidth and with the necessity to perform special tests and measure special characteristics for each new motor prior to utilization.

1. Introduction

A key requirement for sensorless control of an induction motor is the ability to determine the position of the flux in the machine without measuring the speed or position of the rotor. Methods for sensorless control focused on exploitation of saturation effects in a squirrel cage induction motor have been the subject of research in the recent years. These methods can be divided into two groups, depending on whether they use the fundamental excitation of the machine or a separate high frequency excitation. The methods based on fundamental excitation [1-4] fail at low and zero speed, but methods with high frequency excitation do not have such a problem. Methods from the second group can be further divided with regard to the measured signal. This signal can be either the neutral terminal voltage [5], which is less convenient because of the need for additional sensor, or phase currents [6-9], where current sensors already exist, so there is no need for additional hardware. Moreover, there are two different methods that can be used to apply a high frequency signal to the motor. One can utilize either a high frequency signal producing rotating field [6-7] or a high frequency pulsating signal [8-9].

This paper is focused on a method based on injection of a high frequency pulsating voltage vector that rotates in the synchronous *d-q* reference frame and scans the spatial high frequency admittance image. This method allowed one to control the motor torque, but with very limited bandwidth. An injection of a high frequency current signal is also possible, but it demands very fast acting digital current control. Such a fast control becomes increasingly difficult to achieve when the ratio between the sampling frequency and the high frequency signal becomes small.

The traceable saliencies in the motor which appear due to saturation are mainly concentrated in the stator and rotor teeth. The highest saturation occurs along the axis of the rotating flux and changes dynamically with the rate that corresponds to the double fundamental frequency. In other words, the period of the spatial distribution of saliency is equal to one pole pitch of the machine.

In the case when the fundamental voltage (or current) and the high frequency pulsating signal are simultaneously applied the classical model of the induction machine cannot provide useful insight into motor behavior. With FEM analysis a better understanding of the motor behavior under such conditions has been obtained. However, the results of the FEM analysis have demonstrated that because of the variety of motor designs and magnetic non-linearity the suitable control laws could not be designed from conventional motor parameters. Although it has been demonstrated that it is possible to close the torque loop at zero and very low stator frequencies (with very low bandwidth), it is only possible to do so by making special tests on the motor and measure special characteristics which are then used on-line as look-up tables.

All experiments were carried out on a motor: Reliance Electric Company, 3HP, 230/460V, 8.4/4.2 A, 60Hz, 3 phase, 1750 rpm. Since detailed geometric data of the motor necessary for the FE analysis were not available, the simulations were carried out using the data for the motor: Reliance Electric Company, 30 HP, 460 V, 34.6 A, 60 Hz, 3phase, 1765 rpm. The experiments could not be conducted on this particular motor due to the power limit of the available inverter.

2. Method With Injection of High Frequency Pulsating Voltage

The basic principle of this method is to inject a high frequency pulsating voltage signal into the motor and then rotate this pulsating signal in order to obtain a saliency image which is caused by saturation. Since the injected signal is voltage and the measured signal is current, the saliency can be represented by the admittance corresponding to the high frequency signal.

In Fig. 1 the vector diagram presents the principle of this method. The entire processing is performed in the synchronous *d-q* reference frame which rotates with the fundamental frequency. The injected high frequency voltage signal is marked as v_{hf}. This signal is actually a pulsating signal (this is marked with arrows) and could also be represented by two vectors rotating in opposite directions. The angle of this pulsating vector which also rotates with the frequency of 50 Hz relative to the *d-q* frame is marked as ε where $\varepsilon = 2\pi 50t$. The consequence of this injected high frequency voltage signal is the high-frequency current i_{hf_x}, which is pulsating in the direction of the voltage vector v_{hf}. There is also a smaller pulsating current component i_{hf_y} present in the perpendicular direction.

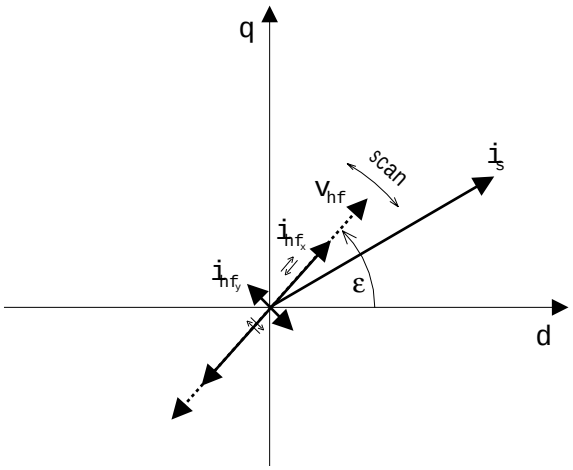

Fig. 1 Vector diagram for pulsating voltage vector injection in *d-q* synchronous reference frame

There are two low-pass filters for the current control loop which decouple the current control of the fundamental signal from the high frequency signal. A band-pass filter is utilized for the high frequency signal processing which transfers only the high-frequency signal and blocks the low frequency.

If the injected pulsating voltage signal also rotates, the measured high frequency current component spatially parallel to the injected voltage changes. Hence, the result is amplitude modulation of the current signal, so that the envelope of the high frequency signal can now be interpreted as the admittance. This signal can be presented in a polar diagram. Figs. 2 and 3 show spatial distribution of admittance for zero torque and torque of +5 Nm, both at zero speed.

An important measurement limitation is that very slow rotation (scanning) of the injected high frequency signal is not very useful because it results in a very slow updating rate. With an appropriate filter design it was experimentally determined that it is possible to increase the scanning frequency of the pulsating vector up to 50 Hz without significant loss of information. With the frequency increase the band-pass filter introduces certain phase shift, but for fixed frequency this phase shift is constant and can be corrected. The phase shift for the 4^{th} order Butterworth band-pass filter with cut-off frequencies 460 Hz and 760 Hz is 22^0. A moving average filter used for amplitude demodulation introduces the additional phase shift of 17.1^0.

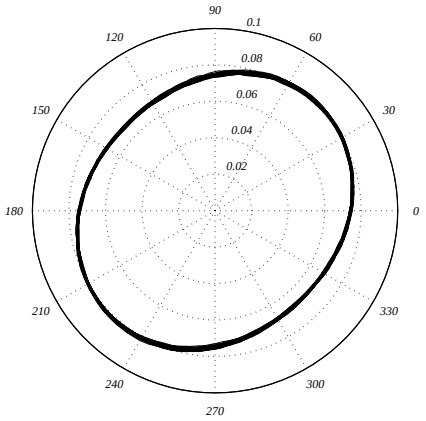

Fig. 2 Measured admittance saliency at scanning frequency 50 Hz for zero torque

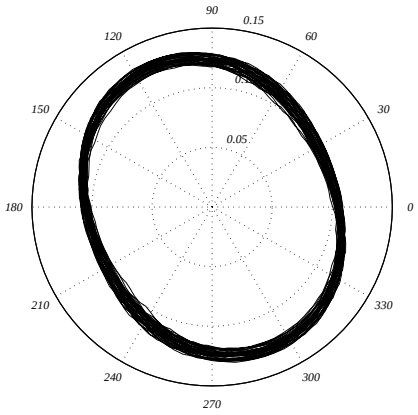

Fig. 3 Measured admittance saliency at scanning frequency 50 Hz for torque +5 Nm

Fig. 4 shows a typical ellipse orientation with stator current vector for positive torque. Angle γ represents the rotation angle of the ellipse, δ is ellipse rotation angle relative to the stator current vector and Y is admittance magnitude. The relationship between the angles γ, δ, the admittance magnitude Y and the torque were measured by test for the steady state condition.

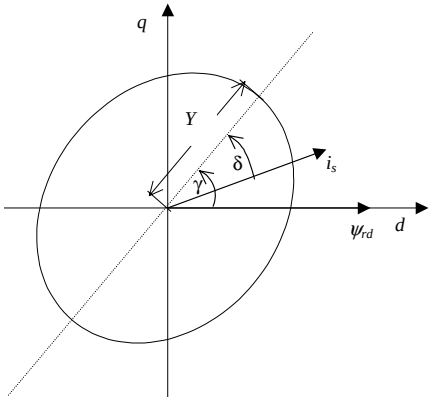

Fig. 4 Ellipse orientation with angles γ, δ and admittance magnitude Y

From the results of steady state measurements shown in Figs. 5 and 6 it is obvious that angles γ and δ are nonlinear functions of torque. These measured steady state data can be used as feedback signals for closed loop torque control. Angle δ was selected as a better candidate for that purpose. Since there always exists a pair of different torque levels which result in only one angle δ, the admittance magnitude Y had to be used as well to form the look-up tables which were then used to calculate estimated torque. The angle γ was not convenient for feedback because the slope of this signal was small for torque levels above ±3 Nm.
Two look-up tables were generated from the results shown in Fig. 6. These two-look-up tables were actually used to calculate estimated torque from previously measured steady state data. The look-up tables are shown in Fig. 7.

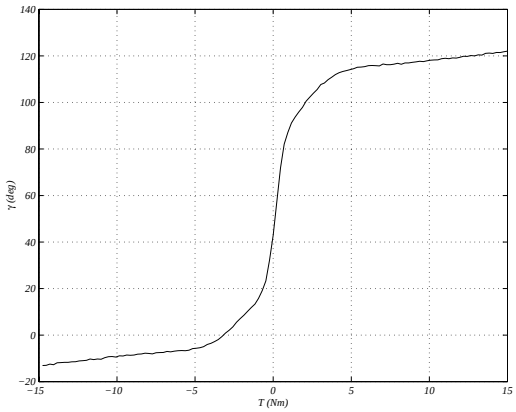

Fig. 5 Relationship between γ and torque

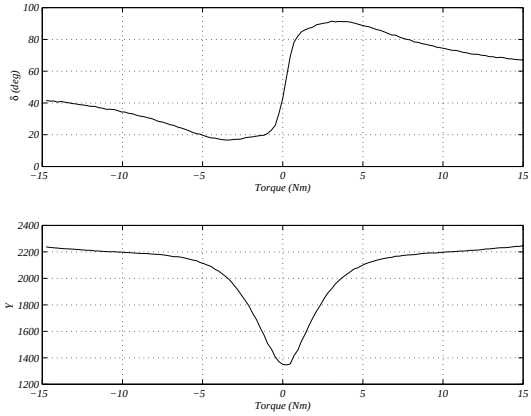

Fig. 6 Relationship between δ, admittance magnitude Y and torque

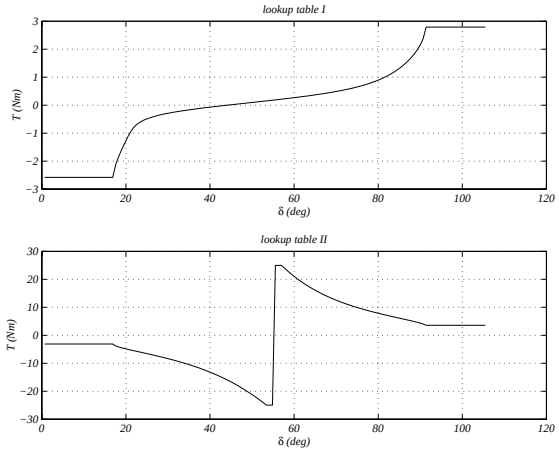

Fig. 7. Look-up tables for torque estimation

An attempt was made to close the loop with only the described torque estimation. In Fig. 8 the proposed control scheme for variable speed sensorless control is presented. The current reference i_{sd}^{ref} is considered as a constant and i_{sq}^{ref} is calculated in the same manner as in the case of indirect rotor flux oriented control. The mechanical rotor frequency ω_m is calculated from the stator frequency ω_e and from estimated slip frequency ω_{sl} as

$$\omega_m = \frac{\omega_e - \omega_{sl}}{p} \tag{1}$$

where p is the number of pole pairs.

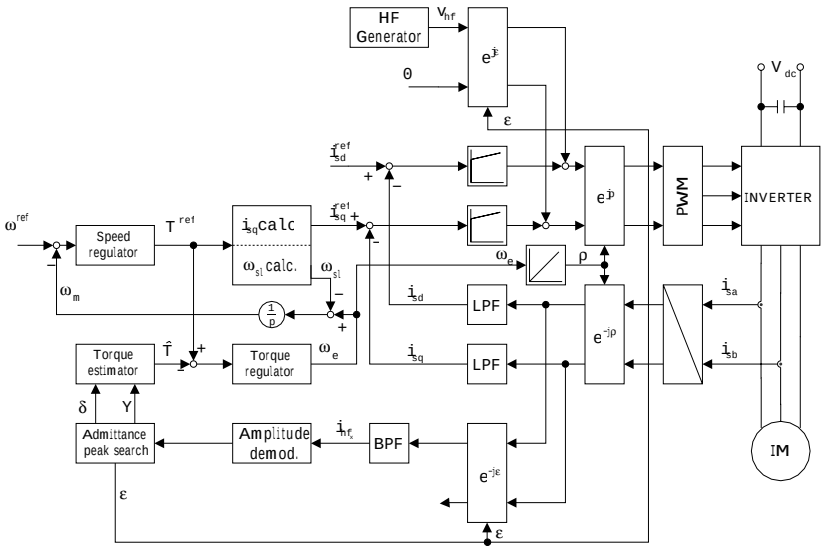

Fig. 8 Proposed control scheme for variable speed sensorless control

The high frequency injection part of the block diagram consists of a high frequency generator that generates the high frequency pulsating signal with constant amplitude 40V and a frequency of exactly one eighth of the sampling frequency $f_{hf} = 610$ Hz (this is important for implementation of amplitude demodulator). Subsequently, this signal is transformed into the *d-q* synchronous reference frame by means of rotational transformation $e^{j\varepsilon}$. Signal injection is then performed in the synchronous reference frame.

The high frequency processing portion starts with the rotational transformation $e^{-j\varepsilon}$ of the current back to the reference frame fixed to the vector of the injected high frequency voltage signal v_{hf} which rotates with the scanning frequency of 50 Hz relative to the synchronous reference frame (see Fig. 1). For processing, only the current component that is collinear with the injected signal is taken into account. After filtering and amplitude demodulation the remaining signal actually represents the admittance. Block marked as "Admittance peak search" basically functions as the maximum detector for admittance and at the same time also outputs the angle δ where the maximum occurs. At the same time this block also generates rotation by the angle ε at 50 Hz. Since there are two maximums per period, values *Y* and δ are updated at the rate of 100 Hz.

The "Torque estimator" contains look-up tables that were obtained by steady state measurements and estimates the torque. The "Torque regulator" is a PI regulator that calculates the stator frequency from the difference between the reference and the estimated torque and attempts to keep this difference equal to zero.

Experimental results for torque mode sensorless control at zero speed with locked rotor are shown in Figs. 9 and 10. The time response of the reference torque, estimated torque, angle δ, admittance magnitude *Y* and slip frequency ω_{sl} are shown. The reference torque has a step change form 0 Nm to10 Nm and then to –10 Nm. The estimated torque contains a strong ripple, but its average value is close to the torque reference. The estimation problem during a step change from 10 Nm to –10 Nm is also very noticeable and is caused by reading from the wrong table because of the bad quality of the signal δ. However, the quality of the estimated torque cannot be better than the quality of angle δ. Hence, in order to improve the quality of the control, the signal δ has to be improved. Despite the poor signal of the estimated torque, the motor generates torque which is close to the reference value. This result can be confirmed by Fig. 10 which shows the slip frequency response. The calculated slip frequency for a

torque of 10 Nm was 7.7 rad/s, so one can observe that the controller generates the proper slip frequency.

One source of the torque ripple is the detection of the angle δ, which is implemented with a simple peak detector at this stage. The other source is the nonlinearity of the inverter, which causes the injected high frequency voltage signal to not possess exactly the desired reference amplitude and angle. The third ripple source could be the motor itself.

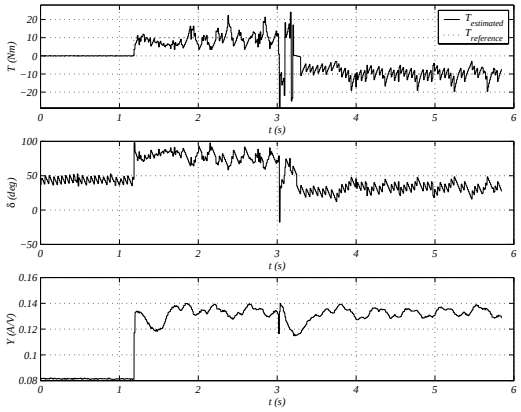

Fig. 9 Closed loop control – Reference torque is changed from 0 Nm to 10 Nm and then to –10 Nm

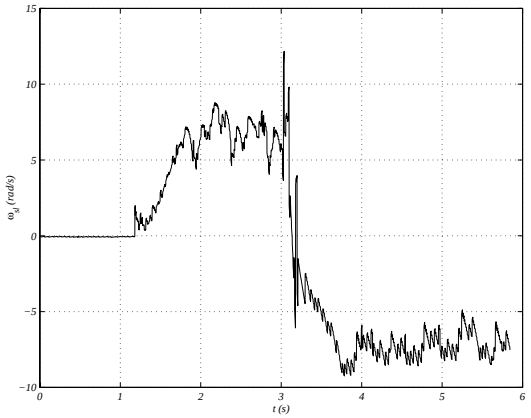

Fig. 10 Closed loop control – step response of slip frequency

Fig. 11 shows the phase current response for a step change of torque from 0 Nm to 10 Nm. The quality of this current waveform is satisfactory. It should be mentioned again that parameters for the torque controller were experimentally determined and the result presented is in the range of the best results obtained with different parameter settings.

Fig. 12 shows typical high frequency waveforms of the phase current for described experiment. A high frequency carrier at 610 Hz can be seen, which has an amplitude modulation of 100 Hz .

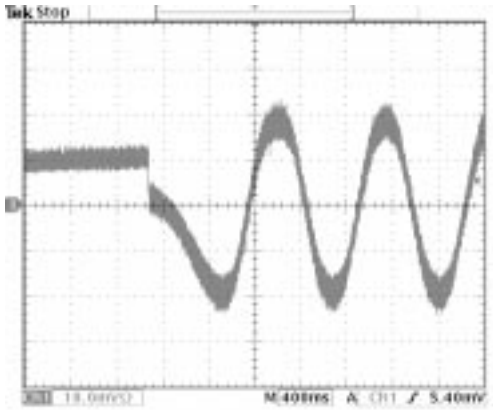

Fig. 11 Closed loop control – phase current (vertical: 5A/div)

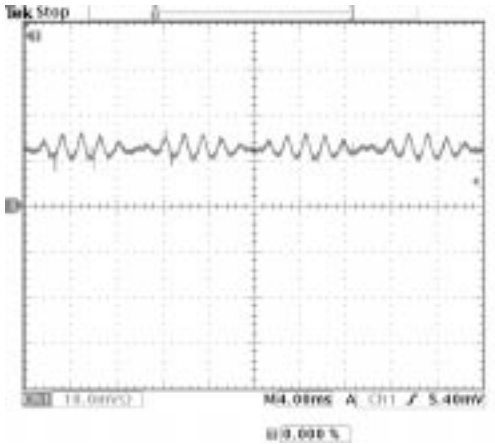

Fig. 12 Phase current - 610 Hz high frequency with 100 Hz amplitude modulation (vertical: 5A/div)

3. Saliency Detection Problem

In the previous section an attempt to close the torque control loop was presented. This section will consider an example of a different 3HP motor (GENERAL ELECTRIC, MODEL 5K182BC218A, 230/460 V, 9/4.5 A, 60 Hz, 1755 rpm) with the same rated power, but from different manufacturer. It

is shown that implementation feasibility for such a control greatly depends on the design of the applied motor.

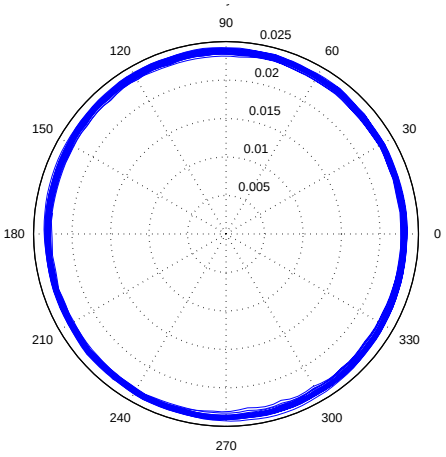

Fig. 13 Admittance saliency for 3HP GE motor

Fig. 13 was recorded for the case of a locked rotor and a torque of +5 Nm and shows the admittance saliency. This result can be directly compared to the result in Fig. 3. It can be seen from Fig. 13 that in contrast to Fig. 3 this particular motor practically shows no admittance change influenced by saturation. Therefore it can be concluded that the proposed method cannot provide useful results in this case. In order to understand this contradictory phenomenon additional research would be required.

4. Finite Element Analysis

Experimental results demonstrated that the position of the minimum inductance obtained from the high frequency component of the armature current does not match well the position of the rotor flux. Moreover, it became apparent that the position of the minimum inductance is a nonlinear function of the torque, so it is almost impossible to predict where the rotor flux will be located only by using the information obtained from the high frequency signal. The finite element method has been used in an attempt to explain this phenomenon.

In order to evaluate these influences a special approach to the FE simulation was taken which allows one to eliminate the influences of fundamental component stator and rotor currents and still obtain the information about the position of the minimum inductance using the envelope of the HF signal. The basic principle is to carry out the simulation for the selected operating point and then “freeze” the distribution of permeances in the nodes of the finite element mesh. These permeances are then used again in a new simulation where only high frequency current is present without the fundamental component. In this way the fundamental component of the flux is eliminated. The HF signal will now scan the machine giving information about the admittance distribution embedded in the nodal values of permeances. To simulate the influence of the squirrel cage, the currents that would normally be induced in the rotor bars due to the HF rotating and pulsating field are replaced by the potential barrier generated by defining Dirichlet’s boundary conditions on the outline of each bar, thus turning their surfaces into equipotential lines. The field generated by the armature currents cannot penetrate the rotor bars because they are now acting as perfect conductors, but without any actual currents flowing through them. Since the fundamental component has been eliminated from the simulation, the voltage sources for all three phases contain only high frequency components that define the voltage vector which rotates with the scanning frequency of 50 Hz and pulsates with the frequency of 500 Hz. The voltage equations are

$$v_{as}(t) = V_{hf}\sin(\omega_{hf}t)\cos(\omega_{sc}t) \tag{2}$$

$$v_{bs}(t) = V_{hf}\sin(\omega_{hf}t)\cos(\omega_{sc}t - \frac{2\pi}{3}) \tag{3}$$

$$v_{cs}(t) = V_{hf} \sin(\omega_{hf} t)\cos(\omega_{sc} t - \frac{4\pi}{3}) \quad (4)$$

where

$f_{sc} = 50$ Hz

$f_{hf} = 500$ Hz

$V_{hf} = 40$ V

The time step used in the transient simulations is T=10^{-4} s. The flux lines of the field simulated in this manner for rated torque (T_R=121 Nm) at zero speed are shown in Fig. 14. The "frozen" permeances used in this simulation were taken from the results of the initial simulation carried out for rated torque at zero speed using only fundamental components of voltages and currents. The results of this initial simulation are shown in Fig. 15. The positions of the armature voltage vector V_{abcs}, armature current vector I_{abcs} and the air gap flux λ_g are also shown in Fig. 15. Armature current waveforms consisting of high frequency components at 500 Hz with an amplitude modulation of 100 Hz are shown in Fig. 16.

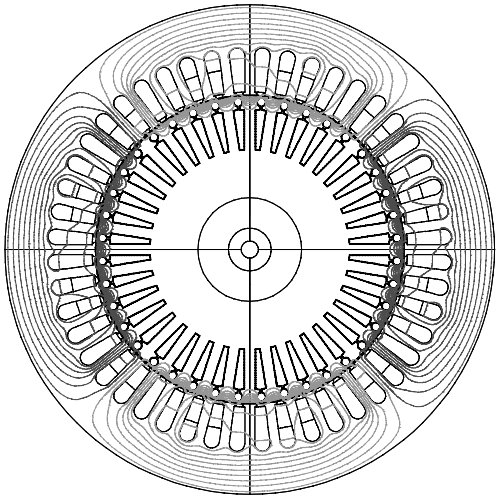

Fig. 14 Flux lines with frozen permeances and rotor bars acting as a potential barrier

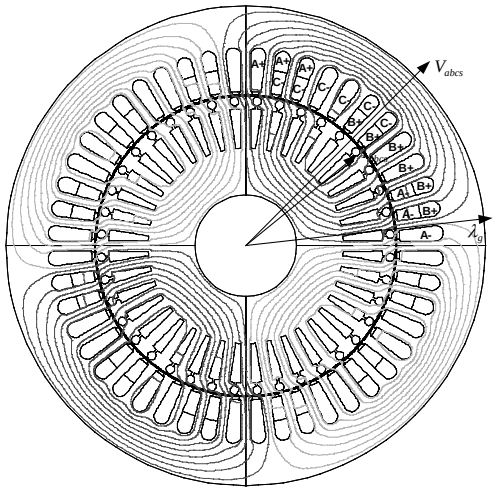

Fig. 15 Flux lines for rated torque (V_s = 8.725 V - phase rms, ω_r= 0, T_R = 121 Nm, f_e = 0.9823 Hz)

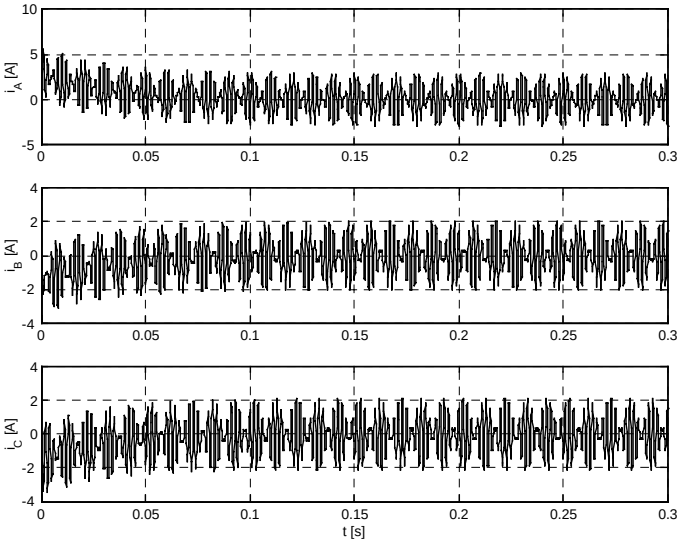

Fig. 16 Simulated armature current waveforms

Since there is no fundamental component in the simulation, only demodulation without filtering can be performed on the simulated armature current waveform. Hence, the ellipse that shows the admittance saliency will be phase shifted by additional 17.1^0. The shape and the position of the ellipse are shown in Figs 17 and 18. The initial 100 ms represents the transient period that exists because the voltages defined by equations (2), (3) and (4) were suddenly applied to the phase windings, so there exists a time period until the armature current reaches steady state. This period should be neglected.

Results of the simulation show that the position of the ellipse is at the angle of 18.6^0 (Fig. 18) which, after subtracting the phase shift of 17.1^0 due to demodulation of the numerically calculated HF current, gives one an angle of 1.5^0. This angle matches the position of the minimum inductance (maximum admittance) shown in Fig. 19. The values of inductance in Fig. 19 were calculated for different positions of the flux vector. The position of the flux vector was varied from $\varphi = -90^0$ to $\varphi = 90^0$ to cover one pole pitch. The angle $\varphi = 0^0$ marks the position of the *q* axis which is also the initial position of the voltage vector as shown in Fig. 15.

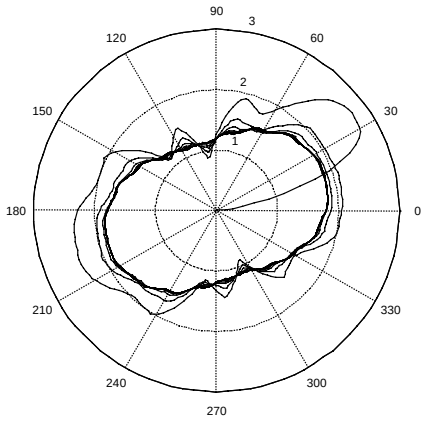

Fig. 17 Simulated envelope of the HF current

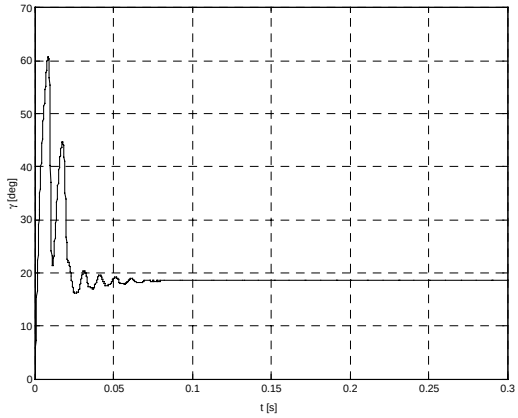

Fig. 18 Position of the envelope relative to the armature voltage

In order to calculate the inductance the first step is to obtain the finite element solution for the selected operating point. The next step is to freeze the permeances and to describe the Dirichlet's boundary conditions on the surfaces of the rotor bars. The angle φ selected between -90^0 and $+90^0$ is marking the position of the current vector. That position, i.e. the angle φ is actually the phase shift of the currents in phases A, B and C relative to the *q* axis. Instantaneous values of phase currents are then given by

$$i_a = I_m \cos(\varphi) \tag{5}$$

$$i_b = I_m \cos(\varphi - 120^0) \tag{6}$$

$$i_c = I_m \cos(\varphi - 240^0) \tag{7}$$

Maximum current I_m can be selected arbitrarily because after freezing the permeances the finite element model becomes linear. The calculated currents i_a, i_b and i_c are now data input for magnetostatic simulation. If these currents are used to form a fixed vector $\underline{i}_{abc}$, the result is a complex number whose absolute value equals I_m and the phase shift is φ.

$$\underline{i}_{abc} = \frac{2}{3}\left(i_a + a i_b + a^2 i_c\right) = I_m \angle \varphi, \; a = e^{j\frac{2\pi}{3}} \tag{8}$$

During post-processing the flux linkages λ_a, λ_b and λ_c are calculated. These flux linkages are used to form the fixed flux vector $\underline{\lambda}_{abc}$ which has the absolute value λ_m and the phase shift φ_λ. The angle φ_λ is different from φ because of the non-uniform distribution of permeances. The flux vector is then

$$\underline{\lambda}_{abc} = \frac{2}{3}\left(\lambda_a + a\lambda_b + a^2\lambda_c\right) = \lambda_m \angle\varphi_\lambda \tag{9}$$

The inductance for the calculated position of the flux is therefore

$$L = \frac{\lambda_m}{I_m}\angle\varphi_\lambda \tag{10}$$

The same procedure is repeated for different values of the angle φ. Fig. 20 shows the values of minimum inductance for different values of torque at zero speed. The shape of the curve that one would obtain after inverting the values of the inductance shown in Fig. 20 is comparable to the shape of the measured curve in Fig. 6 which shows the admittance as a function of torque. These results confirm the assumption that the envelope of the HF component of the current actually shows the position of the minimum inductance, but that position is not the same as the position of the flux. Fig. 21 shows the difference between the position of the ellipse and the position of the air gap flux. The angle of 0^0 in Fig. 21 marks the position of the voltage vector which is also the position of the *q* axis. The experimental results shown in Fig. 5 are comparable with the ones shown in Fig. 21 even though the measurements and simulations were performed on different motors. In order to do quantitative comparison one must subtract the angle of 39.1^0 from the result in Fig. 5 because this is the phase shift due to filtering of the original current signal and demodulation process of the filtered high frequency signal.

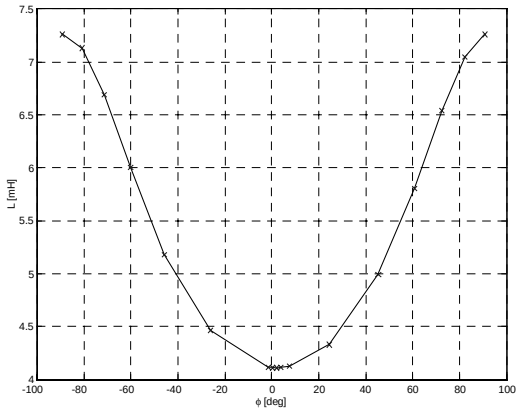

Fig. 19 Inductance distribution for one pole pitch at rated torque and zero speed

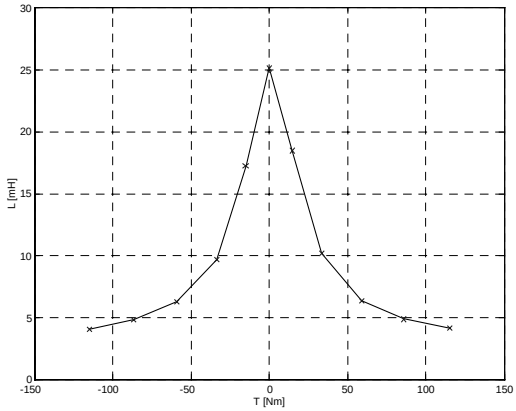

Fig. 20 Minimum inductance for different values of torque at zero speed

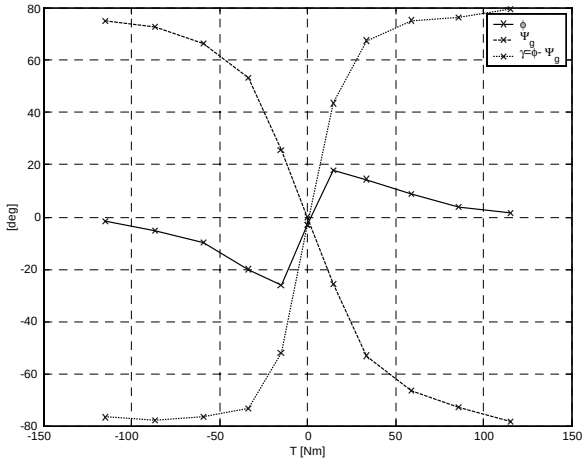

Fig. 21 Positions of the envelope (ϕ) and air gap flux (ψ_g) relative to the armature voltage(0^0) and relative to each other (γ)

Conclusion

Research results concerning sensorless control of an induction motor at zero speed have been presented. The method based on injection of high frequency voltage signal utilizing spatial admittance image tracking has led to useful results where it was possible to close the torque control loop without an encoder at zero speed. The method proved to be capable of controlling the torque, but the dynamics were very poor and the control was not 100% reliable.

For application of this method a series of tests would probably be needed in order to tune the controller for the specific motor (or maybe only the motor type). There is a need for development of an automatic test procedure as a result. Until now all experiments have been done on a 3 HP induction motor with locked rotor. Further research should be done on a motor test bed with torque transducer.

The results of the finite element analysis confirm that the envelope of the HF current is, in reality, showing the position of the minimum inductance. The problem is that the minimum inductance is *not* at the point where the highest saturation in the motor is, i.e. where the air gap flux is positioned. Therefore the position of the minimum inductance is a nonlinear function of torque and this procedure *cannot* be used directly to determine the position of the flux.

The only way to use this method for sensorless control in a closed control loop is to determine in advance the position of the envelope relative to the flux so that an appropriate correction can be carried out on-line. Such a position determination can be either measured or simulated. The main disadvantage of the simulation approach is the duration of the entire process and the necessity to know the detailed geometry of the machine, which in most cases is not available.

Acknowledgments

The authors wish to thank the Allen-Bradley and Reliance divisions of Rockwell Automation for their support during this study.

References

[1] D. S. Zinger, T. A. Lipo, and D. W. Novotny, *Using Induction Motor Stator Windings to Extract Speed Information*, Proc. IEEE-IAS Annu. Meeting, San Diego, CA, Oct. 1989, pp. 213–218

[2] R. M. Cuzner, R. D. Lorenz, and D. W. Novotny, *Application of Nonlinear Observers for Rotor Position Detection on an Induction Motor Using Machine Voltages and Currents*, Proc. IEEE-IAS Annu. Meeting, Oct. 1990, pp. 416–421

[3] A. Ferrah, K. G. Bradley, and G. M. Asher, *Sensorless Speed Detection of Inverter Fed Induction Motors Using Rotor Slot Harmonics and Fast Fourier Transform*, Proc. PESC'92, 1992, pp. 280–286

[4] K. J. Binns, D. W. Shimmin, and K. M. Al-Aubidy, *Implicit Rotor Position Sensing Using Motor Windings for a Self-Commutating Permanent Magnet Drive System*, Proc. Inst. Elect. Eng., vol. 138, Jan. 1991., pt. B, No. 1, pp. 28–34

[5] Alfio Consoli, Giuseppe Scarcella, Antonio Testa, *A New Zero-Frequency Flux-Position Detection Approach for Direct-Field-Oriented-Control Drives*, IEEE Trans. Ind. Applicat., Vol. 36, May/June 2000, No. 3, pp. 797-804

[6] Fernando Briz, Alberto Diez, Michael W. Degner, *Dynamic Operation of Carrier-Signal-Injection-Based Sensorless Direct Field-Oriented AC Drives*, IEEE Trans. Ind. Applicat., Vol. 36, Sep./Oct. 2000, No. 5, pp. 1360-1368

[7] Michael W. Degner, Robert D. Lorenz, *Using Multiple Saliencies for the Estimation of Flux, Position, and Velocity in AC Machines*, IEEE Trans. Ind. Applicat., Vol. 34, Sep./Oct. 1998, No. 5, pp. 1097-1104

[8] Jung-Ik Ha, Seung-Ki Sul, Kozo Ide, Ikuma Murokita, Kohjiro Sawamura, *Physical Understanding of High Frequency Injection Method to Sensorless Drives of an Induction Machine*, Proceedings of IEEE Industry Applications Society, Annual Meeting, Rome, Italy, October 8 – 12, 2000

[9] Jung-Ik Ha, Seung-Ki Sul, *Sensorless Field-Orientation Control of an Induction Machine by High-Frequency Signal Injection*, IEEE Trans. Ind. Applicat., Vol. 35, Jan./Feb. 1999, No. 1, pp. 45-51